DOI: 10.1002/vms3.426

ORIGINAL ARTICLE

WILEY

Two-dimensional and doppler echocardiographic evaluation in twenty-one healthy *Python regius*

Mara Bagardi[1] | Edoardo Bardi[1] | Martina Manfredi[1] | Arianna Segala[1] | Antonella Belfatto[2] | Stefano Cusaro[3] | Stefano Romussi[1] | Paola Giuseppina Brambilla[1]

[1]Department of Veterinary Medicine, University of Milan, Milano, Italy

[2]Department of Electronic, Information and Bioengineering, Politecnico di Milano, Milano, Italy

[3]Ambulatorio Veterinario Associato Cusaro, Merlo, Porati, Pozzoli, Novara, Italy

Correspondence
Stefano Romussi, Department of Veterinary Medicine, University of Milan – via Celoria 10, 20133 Milano, Italy.
Email: stefano.romussi@unimi.it

Abstract

Echocardiographic evaluation is a diagnostic tool for the in vivo diagnosis of heart diseases. Specific and unique anatomical characteristics of the ophidian heart such as the single ventricular cavity, a tubular *sinus venosus* opening into the right atrium, the presence of three arterial trunks and extreme mobility in the coelomic cavity during the cardiac cycle directly affect echocardiographic examination. Twenty-one awake, healthy ball pythons (*Python regius*) were analysed based on guidelines for performing echocardiographic examinations. Imaging in the sagittal plane demonstrated the caudal *vena cava*, *sinus venosus* valve (SVV) and right atrium and the various portions of the ventricle, horizontal septum, left aortic arch and pulmonary artery. Transverse imaging depicted the spatial relationship of the left and right aortic arches, the pulmonary artery and the horizontal septum. Basic knowledge of cardiac blood flow in reptiles is necessary to understand the echocardiographic anatomy. The flow of the arterial trunks and SVV was analysed using pulsed-wave Doppler based on the approach used for humans and companion mammals. The walls and diameters of the *cavum arteriosum*, *cavum venosum* and *cavum pulmonale* were also evaluated. This study should improve the veterinarian's knowledge of ophidian heart basal physiology and contribute to the development of cardiology in reptiles.

KEYWORDS

arterial flows, echocardiography, heart, *Python regius*, snake

1 | INTRODUCTION

In the last few decades, the popularity of snakes (ball pythons in particular) as pets has increased worldwide. From being the prerogative of a few reptile enthusiasts, snakes have come to be considered by many as members of the family, such as with dogs and cats. This has led to a higher demand for high-quality veterinary care for snakes. It is the duty of the reptile specialist to provide it and to bridge this gap in small animal practice. Specifically, echocardiography is an integral part of the cardiac evaluation of humans and domestic animals, but its use is still rarely reported in reptiles, and little emphasis has been placed on ultrasonographic examination of the reptilian heart (Snyder et al., 1999).

Compared with mammals and other reptiles, the ophidian heart exhibits specific and unique anatomical and physiological characteristics. However, ophidians can experience the same diseases,

Mara Bagardi and Edoardo Bardi are equal contributors.

such as endocarditis, myocarditis, infarction, pericarditis, cardiomyopathy, parasitic infestation and tumours (Barten & Frye, 1981; Frye, 1991, 1994; Hruban et al., 1992; Jacobson et al., 1991; Rishniw & Carmel, 1999; Schilliger et al., 2003). Unfortunately, in most cases, the diagnosis of cardiac disease is obtained by post-mortem examination. Cardiovascular diseases in snakes, as well as the match between the anatomy of the heart and two-dimensional ultrasound cross-sectional images, were studied by Sklansky et al. (2001) and Snyder et al. (1999). However, analysis and measurement of the intracardiac and truncal flows with spectral Doppler have never been done. Because of its non-invasive and easily reproducible characteristics, ultrasound examination could be a good option for establishing an in vivo diagnosis of heart disease in reptiles.

The aims of this study were to determine the optimal and reproducible echocardiographic scanning windows with which to measure the cardiac section; to evaluate the intracardiac and truncal flows using the Doppler technique; and to test the intra-operator repeatability of the echocardiographic and Doppler measurements in order to obtain reference values from healthy subjects that can form the basis for the echocardiographic evaluation of cardiac diseases in the ball python (*Python regius*).

1.1 | Reptilian circulation

Blood flow in Pythonidae significantly differs from that of mammals. Variations in blood flow and intracardiac shunts exist in many families of snakes and are also related to environmental conditions (Lillywhite & Donald, 1989; Lillywhite & Gallagher, 1985). Although the snake is described as having a single anatomical ventricle, the ventricle is subdivided into three functional caves. Deoxygenated blood from systemic venous circulation empties into the *sinus venosus*, then enters the right atrium via a bicuspid *sinus venosus* valve (SVV) (Figure 1). Blood is directed from the right atrium through the right atrioventricular (AV) valve into the *cavum venosum*.

During diastole, the *cavum venosum* acts primarily as a channel directing blood into the *cavum pulmonale* (also called the ventral cavum). During systole, *the movement of the horizontal septum allows the blood to flow directly from the cavum pulmonale* towards the pulmonary trunk (Figure 2). A smaller, less developed and incomplete vertical septum subdivides the dorsal *cavum* into the *cavum arteriosum* and *cavum venosum*. Oxygenated blood from the pulmonary veins enters the left atrium and then flows into the *cavum arteriosum*. During systole, due to the plastic activity of the vertical septum, the oxygenated blood is directed from the *cavum arteriosum* through the aortic arches (right and left) passing through the *cavum venosum*.

The AV valves of ophidians are composed of a fibrous medial cusp (Figure 3), and the laterals are absent or rudimentary. The AV valves project into the lumen of the ventricle; in some species, during diastole, they approach the underlying vertical septum. This allows the separation between the *cavum arteriosum* and the *cavum venosum* (Bogan, 2017; Jensen et al., 2010, 2014; Starck, 2009; White, 1968; Wyneken, 2010). During diastole, when the AV valves are open, this morphology helps to direct blood from the atria into the specific ventricular cavities, i.e. from the right atrium to the *cavum pulmonale* and from the left atrium to the *cavum arteriosum*. Consequently, the degree of mixing of oxygenated and deoxygenated blood is quite small (Van Mierop & Kutsche, 1981; Webb et al., 1971). The muscular ridge and the *bulbuslamelle* fuse at the cranial end of the *cavum pulmonale* and *cavum venosum* and connect with the aorticopulmonary septum (dividing the pulmonary artery from the two aortas) (Goodrich, 1919; Jensen et al., 2014). The structural specialization

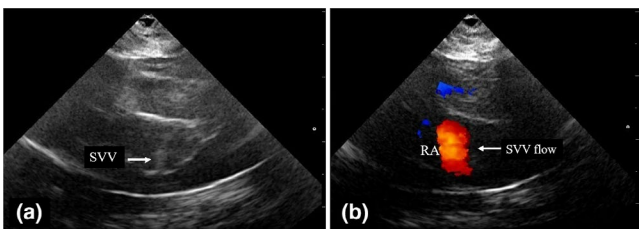

FIGURE 1 Detail of the *sinus venosus* valve (SVV). (a) The medial sagittal section at this level allows an optimal visualization of the SVV (closed in the image). (b) The application of colour Doppler allows the identification of the blood flow (red) from the *sinus venosus* to the right atrium (RA) through that SVV

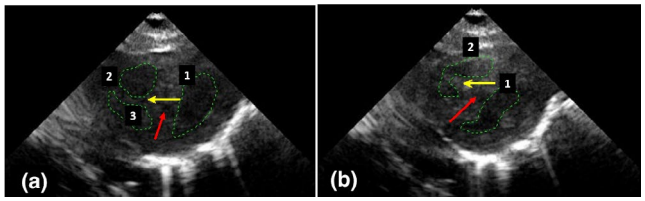

FIGURE 2 Trans-ventricular short-axis section, showing the ventricular cava and the movements of the horizontal septum (yellow arrow). 1: *cavum arteriosum*; 2: *cavum pulmonale*; 3: *cavum venosum*. (a) during systole the horizontal septum contracts, allowing the separation between the *cavum venosum* and the *cavum pulmonale*. (b) during diastole the horizontal septum is relaxed, and the two cava communicate. In both phases of the cardiac cycle, it is evident how the vertical septum (red arrow) contributes to the separation of the cava

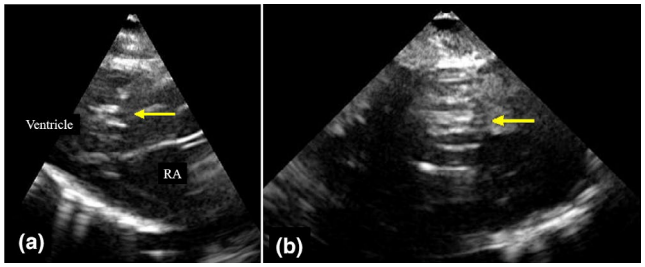

FIGURE 3 Detail of the atrioventricular valve (AVV). (a) Medial sagittal section of the ventricle optimized to observe the AVV (yellow arrow) while open during diastole; RA: right atrium. (b) From the previous scan (a), rotating the probe by 90°, it is possible to obtain the visualization of the AVV in the short axis. In this section, the RA is located dorsally at the AVV towards the observer

of the ventricle ensures a complete separation of flows and pressures between the systemic and pulmonary circles; this system is called the "*double pressure pump*" (Jensen et al., 2014; Jensen & Nyengaard, 2010; Wang et al., 2003). In these species (Pythonidae), *the left heart*, *formed in systole by the cavum arteriosum* and *cavum venosum*, acts as a high-pressure chamber and constitutes, with its thick muscular wall, approximately 75% of the heart mass, while the *cavum pulmonale* acts as a low-pressure chamber and constitutes the remaining 25% (Jensen et al., 2014; Jensen & Nyengaard, 2010).

Due to this peculiar ventricular anatomy, the right-left and left-right shunts may appear under certain physiological conditions as well as a consequence of alterations in systemic and pulmonary pressures.

The small shunts, which are also physiologically present in this species, depend less on peripheral resistance in the two circles. They depend more on the volume of the *cavum venosum* and less on the volume from the *cavum arteriosum*. For this reason, shunts are not particularly frequent in pythons as compared with other snake and reptilian species and are mainly of the left-to-right variety ("washout shunts") (Bogan, 2017; Jensen et al., 2010, 2014; Jensen & Nyengaard, 2010). The few shunts evidenced in pythons, however, reveal a certain efficiency in keeping systemic and pulmonary flows separate even in diastole. This has been put in relation with the downward opening movement of the AV valves towards the vertical *septum* (Bogan, 2017; Jensen et al., 2010, 2014; Jensen & Nyengaard, 2010).

2 | MATERIALS AND METHODS

The study was conducted on privately owned *P. regius* prospectively recruited at the Exotic Animal Medicine Unit of the University Veterinary Hospital (Department of Veterinary Medicine, University of Milan–Lodi) between December 2018 and June 2019. Informed consent was signed by the owners, according to the University of Milan Ethics Committee Statement Number 2/2016.

To ensure the standardization of the physiological parameters, the snakes were individually housed in 120 × 80 × 60 cm glass cages with water ad libitum and shelter for 7 days at a standard temperature (26–30°C) and humidity (50%–70%). Their diet consisted of thawed or freshly killed prey (mice and rats) provided once a month. The snakes had been fasting for at least 1 month prior to measurement to assure that they were in a post-absorptive condition.

For each snake, we collected clinical data (reporting and history) and carried out a general clinical examination, chest radiography examination and full echocardiographic examination. The *P. regius* subjects selected were clinically healthy, in good physical condition and had no external or internal parasites and no injuries. Owing to these characteristics and to the absence of clinical symptoms related to cardiovascular problems, we classified these subjects as normal, despite the lack of a post-mortem examination to confirm it. Subjects that displayed any alteration during physical examination, active ecdysis or that had been fed in the previous 15 days were not included in the study.

Direct digital radiographies of the coelomic cavity at the cardiac projection area were performed using standard latero-lateral and dorso-ventral projections at 60 kV and 13 mA (Divers & Mader, 2006). Echocardiographic examination (2-D, M-mode, spectral and colour-flow Doppler) was performed using a MyLab50 Gold cardiovascular ultrasound machine equipped with a multi-frequency phased array probe (7.5–10 MHz). Each snake was examined while manually restrained in a dorsally recumbent position and under the standard environmental conditions proposed by the literature, i.e. a temperature of 23–28°C and a humidity of 50%–70% (Barten & Frye, 1981; Schilliger et al., 2006; Snyder et al., 1999). Ultrasound gel was applied for coupling the scanner head to the ventral scales of the snakes. The probe was set to 10 MHz with a pulse repetition frequency of 32 frames/s and 40% gain. High-quality video clips were acquired and stored using echo machine software for off-line measurements.

The examination and two-dimensional Doppler measurements were carried out by a single operator (MB). All measurements of interest were repeated on three consecutive cardiac cycles and on three different days. The obtained data were subjected to statistical analysis as reported by Conceicão et al. (2014). The two-dimensional echocardiographic projections used to obtain the measurements are shown in Figure 4. The thickness of the septa and the walls of the cava, as well as their diameters, were measured using the leading-edge to leading-edge method (Mattoon & Nyland, 2015).

The echocardiographic windows used to execute the colour and spectral continuous-wave (CW) and pulsed-wave (PW) Doppler evaluation were the trans-arterial long-axis view, obtained at the base of the heart. They were optimized to measure the blood flow throughout the *cavum pulmonale* into the pulmonary artery and from the *cavum venosum* into the two aortas through the respective semilunar valves (Starck, 2009). The velocities and gradients of the AV flows were not evaluated because it is not possible to obtain the correct alignment of the blood flow through the AV valves and the ultrasound beam. Ultrasound software was used to calculate the average, peak velocity and gradients of the detected flows. The heart rate of each animal was calculated from PW Doppler images.

2.1 | Study design and statistical analysis

Statistical analysis was performed using SPSS™ 25.0 (IBM, SPSS). Each measurement was repeated three times on different days. The normal distribution was assessed using the Shapiro-Wilk test. The analysed variables are normally distributed, and data are reported as the mean and standard deviation.

Descriptive analysis provided the physical and echocardiographic parameters of the population. Correlations between each flow measure and the physical characteristics of the animals were analysed. The Pearson's correlation index tested the simple linear correlation between two variables. The Pearson's coefficient

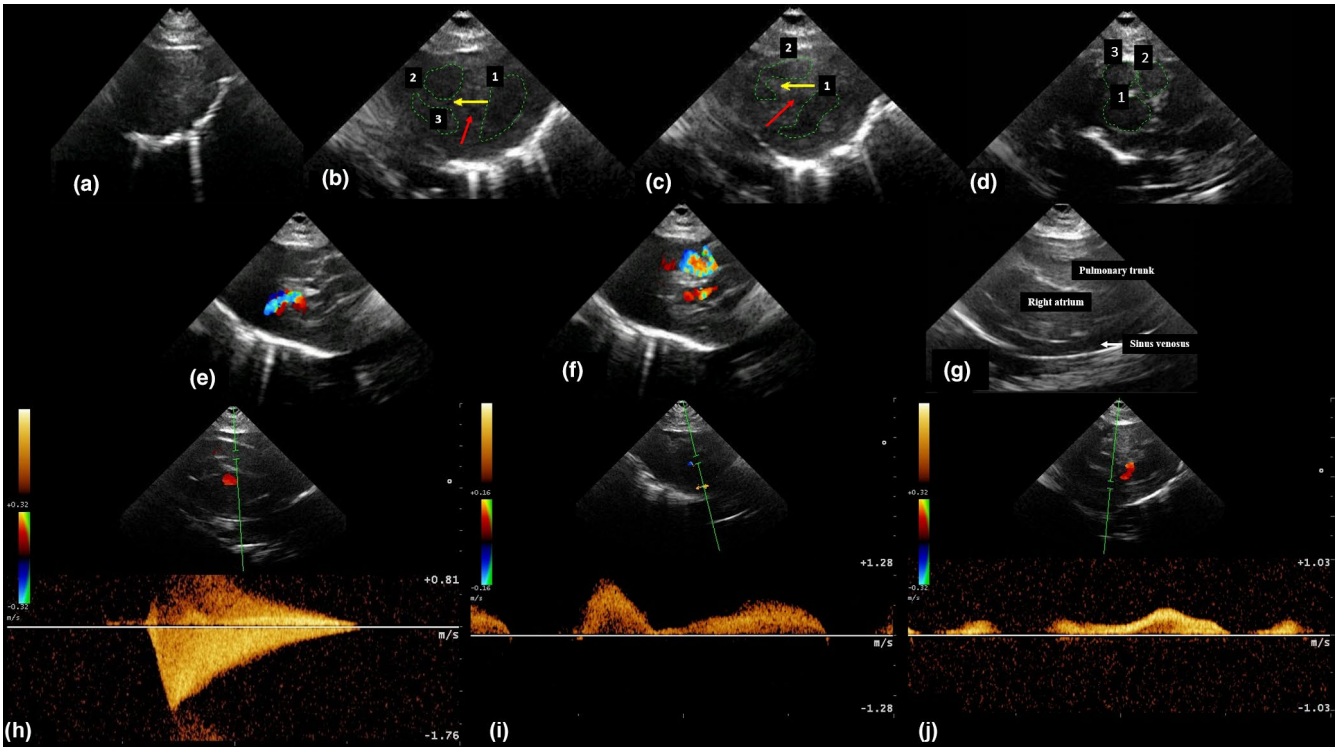

FIGURE 4 Two-dimensional echocardiographic projections used to obtain the short axis, long axis and Doppler measurements. (a) Apical diastolic short-axis section, showing a transversal view of the ventricular apex enabling the observation of the spongy nature of the ventricular myocardium. (b, c) Trans-ventricular short-axis section, showing the ventricular cava and the movements of the horizontal septum (yellow arrow) and vertical septum (red arrow) in systole and diastole. 1: *cavum arteriosum*; 2: *cavum pulmonale*; 3: *cavum venosum*. (d) Trans-arterial short-axis section in diastole. This section shows the emergence of the three arterial trunks and makes possible the measurement of their diameters. 1: pulmonary artery; 2: left aorta; 3: right aorta. (e, f) Median longitudinal ventricular section at the level of atrio-ventricular valve (AVV) in diastole and systole, respectively. The application of colour Doppler makes possible the visualization of the blood flow and heart structures during the different phases of the cardiac cycle. (e) Late-phase diastole. The image shows the complete filling of the *cavum arteriosum* in diastole, while it is not possible to highlight the flow from the *cavum venosum* through the *cavum pulmonale*. (f) Ventricular systole. Colour Doppler shows the blood flowing from the *cavum pulmonale*, at the top of the image, to the pulmonary trunk and from the *cavum venosum* to the two aortas. (g) Medial cranial sagittal section at the *sinus venosus* valve (SVV) level. This section shows, in ventral position, the caudal *vena cava* contributing to the formation of the *sinus venosus* (white arrow) that opens in the right atrium through the SVV. Dorsal in the image, the emergence of the pulmonary trunk, dorsally to the right atrium, is evident. (h) The trans-arterial long-axis section for the evaluation of the pulmonary blood flow. The use of PW Doppler in this section, pointing the marker on the pulmonary trunk, permits the evaluation of the blood flow through the semilunar pulmonary valve in systole. (i) Trans-arterial long-axis section and evaluation of the aortic blood flow. The use of PW Doppler in this section, pointing the marker on the aortic bifurcation, permits the evaluation of the blood flow passing through the two semilunar valves towards the aortas in systole. (j) Medial sagittal section of the SVV. The use of PW Doppler on this section permits the evaluation of the blood flow through the SVV

(*R*-coefficient) is interpreted as follows: 0.3 = weak correlation, >0.3 and <0.7 = moderate correlation and >0.7 = strong correlation. The repeatability of echocardiographic measurements was determined using the Friedman test. A parameter was considered repeatable if it had a significance value >5%. The 95% confidence interval was considered, and differences were defined as statistically significant at $p < 0.05$.

3 | RESULTS

Twenty-four animals were visited, of which 21 met the inclusion criteria and were included in the study. The ages were between 2 and 20 years (average 6.5), weight ranged from 0.475 to 2.015 kg (mean ± *SD* 1.39 ± 0.46 kg) and length ranged from 76 to 131 cm (mean ± *SD* 110.78 ± 14.36; nose-to-cloaca). The population was 36.8% female and 63.2% male and included subjects of any morph, in particular: 42.1% ancestral, 15.8% albino, 10.5% yellow belly and other morphs represented in lower percentages.

3.1 | Radiographic examination

Radiographic examination of the cardiac projection proved to be very difficult due to the absence of air around the heart itself, which is located inside the coelomic cavity and placed cranially in relation to the lungs, making the normal contrast evidenced in mammals infeasible in the case of pythons. No animals were subjected

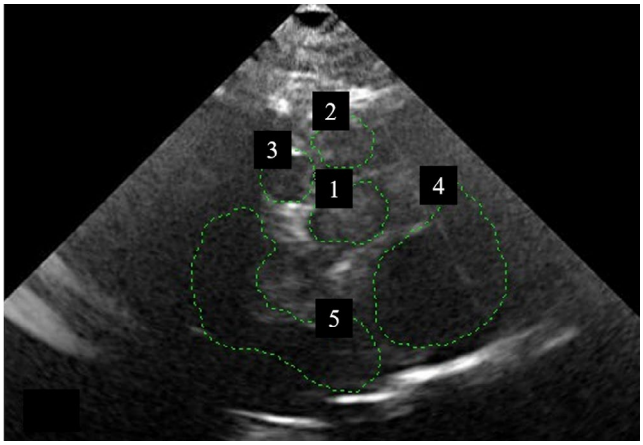

FIGURE 5 Trans-arterial short-axis section. This scan makes possible the observation of the two atria. 1: pulmonary artery; 2: left aorta; 3: right aorta; 4: left atrium; 5: right atrium

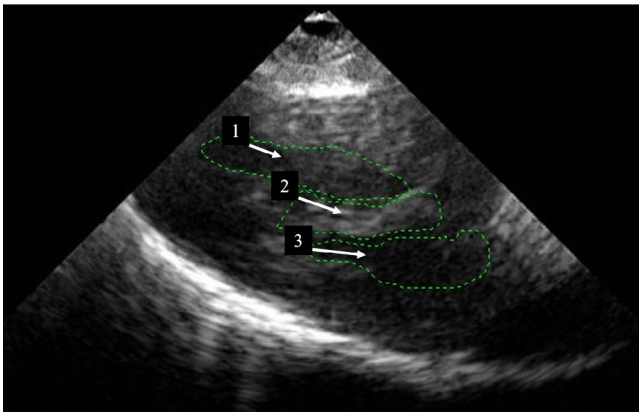

FIGURE 6 Median sagittal section of the ventricle during diastole. This scan allows for the visualization of the *cavum pulmonale* and *cava arteriosum* in long axis, the walls of the ventricle, the movement and the thickness of the vertical and horizontal septa and the opening–closing movements of the atrio-ventricular valve (AVV). 1: *cavum pulmonale*; 2: muscular ridge; 3: *cavum arteriosum*

to pharmacological restriction. Therefore, in some cases, perfect positioning in the *latero-lateral* and *dorso-ventral decubitus* was remarkably difficult.

3.2 | Two-dimensional echocardiography

For all subjects, it was possible to obtain images of acceptable quality. The docile nature of these animals allowed us to carry out all echocardiographic examinations without difficulty. Even in the smallest subjects, it was possible to evaluate all the investigated cardiac structures. A ventral approach with transverse orientation of the probe allowed us to obtain cross-sectional images of the ventricle, the atria (Figure 5) and the major vessels (Figure 4d). From the apex of the heart to the root of the major vessels, the extension and position of the chambers and the septa (horizontal septum and muscular ridge) were viewed (Figure 4a-c). The dimensions of the cava were measured at the same distance from the apex to the outflow tract of each cava. The *cavum venosum* occupied the ventrocranial part of the ventricle and was partially continuous with the interventricular canal. The *cavum arteriosum* was separated from the two other caves by the horizontal septum (also called the interventricular septum). The *cavum pulmonale* and *cavum venosum* were partially separated by the muscular ridge (Figure 6). This was a prominent structure better visualized in cross section, close to the base of the ventricle. Moving the probe cranial to the muscular ridge, the root of the major vessels can be visualized. The left and right aortas originate next to each other from the *cavum venosum* in a ventral-right position and have approximately the same cross-sectional diameter. The *truncus pulmonalis* originates from the *cavum pulmonale* in a ventral-left position and is well separated from both aortas. The cross-sectional diameter of the *truncus pulmonalis* is larger than the diameter of the aortas. In the cranial position, pulmonary trunk separation into the left and right pulmonary arteries was observed.

The mean, standard deviation and minimum and maximum values of each two-dimensional echocardiographic parameter were calculated and are summarized in Tables 1 and 2. Even if the *R*-coefficients are not very high, the *p*-values were <0.05. All positive and negative correlations are reported in Supplementary Information 1 and 2.

Intra-operator repeatability of the short-axis measurements was evaluated: all measurements were repeatable and no statistically significant differences were evidenced ($p > 0.05$) except for the systolic and diastolic diameters of the vertical septum (2% and 4.5%, respectively), the diastolic thickness of the *cavum arteriosum* (1.3%), the systolic diameter of the *cavum pulmonale* (0.7%) and the systolic thickness of the free wall of the *cavum arteriosum* (4.3%). Furthermore, the long-axis measurements that were not reliable (i.e. not repeatable) were the diastolic diameter of the *cavum pulmonale* (1.1%), the thickness of the horizontal septum in diastole (3.3%), the systolic diameter of the *cavum arteriosum* (3.9%) and the thickness of the free wall of the *cavum arteriosum* (2.2%; Supplementary Information 3 and 4).

3.3 | Doppler echocardiography

Cranially to the pulmonary trunk, the aortas bend dorsally: first the left and then the right vessels. Starting from the right aorta, the brachiocephalic artery branches just before it bends dorsally. The best visualization of the bending of the aortas was obtained with the probe in longitudinal position and the transducer oriented in order to adjust the differences in the topography of the vessels. As the two aortas curve dorsally, it was easier to orient the ultrasound beam parallel to the blood flow and therefore perform the Doppler measurements. Orienting the probe longitudinally and laterally, both the pulmonary and aortic flows were identified (Figure 4h,l). The right atrium, the *cavum arteriosum*, the *cavum venosum*, the AV valves

TABLE 1 Descriptive statistics of short-axis echocardiographic parameters considered in the study

Short axis	DVØ Vd (mm)	LLØ Vd (mm)	Ø CPd (mm)	Ø Cad (mm)	Ø CVd (mm)	CPWd (mm)	HSd (mm)	VSd (mm)	CAWd (mm)	Ø CPs (mm)	Ø Cas (mm)	Ø CVs (mm)	CPWs (mm)	HSs (mm)	VSs (mm)	CAWs (mm)	Ø Pas (mm)	Ø lAos (mm)	Ø rAos (mm)
Mean	8.95	9.96	2.74	3.96	2.38	1.77	2.08	2.19	2.49	1.87	2.61	2.12	1.61	2.07	2.44	3.01	4.82	3.11	3.32
SD	2.25	2.39	0.79	1.22	1.59	0.49	0.46	0.55	0.37	0.37	0.77	0.66	0.32	0.45	0.61	0.72	1.53	0.83	0.84
Minimal	6.00	7.00	1.40	2.30	0.09	1.00	1.30	1.40	1.70	1.00	1.10	1.00	1.20	1.10	1.60	1.90	2.10	1.60	1.60
Maximum	13.70	15.30	4.40	6.60	6.60	2.70	3.10	3.70	3.20	2.70	4.00	3.30	2.40	2.90	3.70	4.50	8.70	4.70	4.50

Abbreviations: CAWd, thickness of the wall of the *cavum arteriosum* during diastole; CAWs, thickness of the wall of the *cavum arteriosum* during systole; CPWd, thickness of the wall of the *cavum pulmonale* during diastole; CPWs, thickness of the wall of the *cavum pulmonale* during systole; DVØ Vd, dorso-ventral diameter of the ventricle during diastole; HSd, horizontal septum during diastole; HSs, horizontal septum during systole; LLØ Vd, latero-lateral diameter of the ventricle during diastole; Ø Cad, diameter of the *cavum arteriosum* during diastole; Ø Cas, diameter of the *cavum arteriosum* during systole; Ø CPd, diameter of the *cavum pulmonale* during diastole; Ø CPs, diameter of the *cavum pulmonale* during systole; Ø CVd, diameter of the *cavum venosum* during diastole; Ø CVs, diameter of the *cavum venosum* during systole; Ø lAos, diameter of the left aorta during systole; Ø Pas, diameter of the pulmonary artery during systole; Ø rAos, diameter of the right aorta during systole; *SD*, standard deviation; VSd, vertical septum during diastole; VSs, vertical septum during systole.

TABLE 2 Descriptive statistics of the long-axis echocardiographic parameters considered in the study

Long axis	Ø CPd (mm)	Ø Cad (mm)	Ø CVd (mm)	CPWd (mm)	HSd (mm)	VSd (mm)	CAWd (mm)	Ø CPs (mm)	Ø Cas (mm)	Ø CVs (mm)	CPWs (mm)	HSs (mm)	VSs (mm)	CAWs (mm)	SVV (mm)	tØ rAt (mm)	Ø PA (mm)	Ø lAo (mm)
Mean	2.39	2.97	1.87	1.63	2.10	2.61	2.78	1.91	2.54	2.65	1.84	2.24	2.43	2.86	2.59	6.30	3.81	3.18
SD	0.97	0.86	0.77	0.44	0.77	1.00	0.60	0.72	0.76	0.50	0.45	0.53	0.64	0.58	0.58	1.84	0.92	0.99
Minimal	1.30	1.30	1.10	1.20	1.10	1.20	1.90	1.10	1.30	1.90	1.10	1.60	1.30	1.70	1.70	3.90	2.70	1.70
Maximum	4.50	4.80	4.00	2.90	3.80	5.00	4.40	3.40	4.20	3.40	2.80	3.40	3.90	4.00	3.90	9.70	5.50	5.60

Abbreviations: CAWd, thickness of the wall of the *cavum arteriosum* during diastole; CAWs, thickness of the wall of the *cavum arteriosum* during systole; CPWd, thickness of the wall of the *cavum pulmonale* during diastole; CPWs, thickness of the wall of the *cavum pulmonale* during systole; HSd, horizontal septum during diastole; HSs, horizontal septum during systole; Ø CAd, diameter of the *cavum arteriosum* during diastole; Ø CAs, diameter of the *cavum arteriosum* during systole; Ø CPd, diameter of the *cavum pulmonale* during diastole; Ø CPs, diameter of the *cavum pulmonale* during systole; Ø CVd, diameter of the *cavum venosum* during diastole; Ø CVs, diameter of the *cavum venosum* during systole; Ø lAo, diameter of the left aorta; Ø PA, diameter of the pulmonary artery; *SD*, standard deviation; SVV, opening of the *sinus venosus* valve; tØ rAt, transversal diameter of the right atrium; VSd, vertical septum during diastole; VSs, vertical septum during systole.

TABLE 3 Descriptive statistics of Doppler echocardiographic parameters considered in the study

Doppler	FVI PA (m)	mV PA (m/s)	mG PA (mmHg)	pV PA (m/s)	pG PA (mmHg)	FVI SVV (m)	pV SVV (m/s)	pG SVV (mmHg)	mG SVV (mmHg)	Dur SVV (s)	FVI lAo (m)	mV lAo (m/s)	mG lAo (mmHg)	pV lAo (m/s)	pG lAo (mmHg)	FVI rAo (m)	pV rAo (m/s)	pG rAo (mmHg)	mG rAo (mmHg)
Median	0.23	−0.36	0.77	−0.78	2.65	0.19	0.30	0.38	0.16	1.11	0.14	0.48	1.22	0.83	2.13	0.20	0.42	0.72	0.37
SD	0.08	0.08	0.36	0.21	1.298	0.08	0.06	0.15	0.07	0.45	0.07	0.18	0.99	0.69	1.36	0.04	0.09	0.29	0.14
Minimal	0.16	−0.53	0.30	−1.23	0.90	0.07	0.20	0.20	0.10	0.46	0.04	0.15	0.10	0.24	0.20	0.11	0.25	0.30	0.10
Maximum	0.50	−0.21	1.60	−0.20	6.00	0.39	0.44	0.80	0.30	2.01	0.42	1.08	5.10	3.70	6.40	0.38	0.58	1.30	0.70

Abbreviations: Dur. SVV, duration of the flow through the *sinus venosus* valve; FVI lAo, velocity integral of the flow through the left aorta; FVI PA, velocity integral of the flow through the pulmonary artery; FVI rAo, velocity integral of the flow through the right aorta; FVI SVV, velocity integral of the flow through the *sinus venosus* valve; mG lAo, mean gradient of the flow through the left aorta; mG PA, mean gradient of the flow through the pulmonary artery; mG rAo, mean gradient of the flow through the right aorta; mG SVV, mean gradient of the flow through the *sinus venosus* valve; mV lAo, mean velocity of the flow through the left aorta; mV PA, mean velocity of the flow through the pulmonary artery; pG lAo, peak gradient of the flow through the left aorta; pG PA, peak gradient of the flow through the pulmonary artery; pG rAo, peak gradient of the flow through the right aorta; pG SVV, peak gradient of the flow through the *sinus venosus* valve; pV lAo, peak velocity of the flow through the left aorta; pV PA, peak velocity of the flow through the pulmonary artery; pV rAo, peak velocity of the flow through the right aorta; pV SVV, peak velocity of the flow through the *sinus venosus* valve; *SD*, standard deviation.

and the interventricular canal were also observed. Moreover, this echocardiographic window allowed the analysis of the blood flows through the ventricle in systole as well as the AV valves, but not the movement of the muscular ridge (Figure 4e,f). Flows through the AV valves were analysed using colour Doppler, which highlighted a laminar pattern. The impossibility of parallel alignment to these flows prevented their correct evaluation with pulsed Doppler. Despite the wide cranio-caudal movement of the heart in the coelomic cavity during the cardiac cycle, the velocity and ejection time in the left aorta were reliable and easily repeatable. The evaluation of the flow in the right aorta resulted in an overestimation of ejection time due to the persistence in time of the Doppler sample volume within the vessel secondary to the caudal cranial movement of the heart associated with a low heart rate. It is necessary to underline that a certain degree of interindividual variability in the anatomy of the major vessels existed.

The mean, standard deviation and minimum and maximum values of the PW Doppler parameters were analysed and are summarized in Table 3. Mean FVI (flow velocity integral) of the pulmonary artery, both aortas and the SVV was low, i.e. between 0.14 and 0.23 m. Echocardiographically, all Doppler blood flows were laminar with low velocity. Compared with the pulmonary artery and both aortas, SVV flow had the longest duration (1.11 ± 0.45 s, ranging from 0.46 to 2.01 s). CW Doppler was not useful for echocardiographic examination given the low physiological flow rate of this species.

Pearson's analysis and the correlation among the Doppler variables are shown in Supplementary Information 5. Pulmonary mean velocity was slightly negatively correlated with body weight ($r^2 = -0.263$), whereas the peak velocity of the left aorta was positively correlated with body weight ($r^2 = 0.274$). Peak velocity of the SVV was moderately correlated with body length ($r^2 = 0.312$). Many other significant positive correlations were identified (*R*-coefficient >0.7) between Doppler measurements. Intra-operator repeatability was evaluated by repeated Doppler measurements. No statistical differences were observed ($p > 0.05$; Supplementary Information 6).

4 | DISCUSSION

The ball python is one of the most studied snake species in terms of cardiac anatomy and physiology (Jacobson et al., 1991; Schilliger et al., 2003; Snyder et al., 1999). Despite the presence of reports referring to congenital or acquired heart disease evidenced in the context of autopsy, (Schilliger et al., 2003, 2010) scientific literature regarding in vivo identification of heart disease in reptiles by echocardiographic examination is still poor (Schilliger et al., 2010; Young & Saunders, 1999). In fact, very few studies employ Doppler techniques to visualize and quantify blood flows throughout the AV valves and, to our knowledge, no investigations on the morphology and measurement of the velocity of outflow tracts have been performed using spectral Doppler (Hochscheid et al., 2002; Starck, 2009; Starck & Wimmer, 2005; Young & Saunders, 1999). Moreover, a reference interval has yet to be described for the Doppler measurement of outflow tracts.

Despite the small size of the subjects of this species, which sometimes did not allow excellent quality images to be obtained, our study demonstrates the feasibility of the ultrasonographic technique as a non-invasive tool to study the functional anatomy of the python heart. The reproducibility of the echocardiographic-obtained images and the repeatability of the linear measurements as well as of the intracardiac flows were significantly high. The standard echocardiography images obtained from the transverse plane at the level of the interventricular canal, and from the horizontal longitudinal plane including the atria, the *cavum arteriosum*, the *cavum venosum* and the AV valves were useful to evidence the majority of structures (Snyder et al., 1999). Moreover, the additional oblique plane applied in our study provided a better visualization of the left atrium, the cranial *vena cava* and the septa. The proposed oblique orientation of the transducer, orienting the probe longitudinally and laterally on the left side of the snake, allowed the correct alignment of the ultrasound beam and the blood flow in the pulmonary trunk and the two aortas.

The longitudinal imaging plane showed that the filling of the pulmonary artery precedes the filling of the aortas. Furthermore, the timing of the action of the AV valves and the muscular ridge is the key feature that allows for the shunting of blood between systemic and pulmonary circulation. The dual-pressure system reported for the circulation in *P. regius* can be explained by the cranio-caudal motion of the muscular ridge, and the consequence is the different timing of the pulmonary and both aortic outflows (Wang et al., 2002, 2003). The Doppler method showed that the muscular ridge separates blood flows in the *cavum pulmonale* and the *cavum venosum*, and the closure between the *cavum venosum* and the *cavum pulmonale* is so tight that the pulmonary and systemic circulations run at different pressures (the double-pressure pump).

Some limitations emerged during this study. Contrary to what has been reported previously, (Divers & Mader, 2006). X-ray radiographic examination of the cardiac projection area was of little use in the identification of reference parameters in healthy subjects. This is because, with the animal being conscious, the correct positioning was difficult to obtain, and the highlighting of the cardiac structures was not particularly accurate due to the obliquity of the obtained radiographic scans.

Regarding the ultrasound, the disproportions between the size of the snakes and the tip of the transducer meant that we did not always obtain high-quality images. Furthermore, the frame rate of the ultrasound machine (Esaote MyLab50 Gold Cardiovascular) used in this study did not provide the appropriate temporal resolution to identify the opening of the interventricular canal and the closing of the muscular ridge at the same frame. The extremely trabecular nature of the ventricle, the wide motion of the septa and the cranio-caudal movement of the heart into the coelomic cavity make the M-mode technique unreliable in snakes.

A lack of repeatability was observed for the long-axis diastolic diameter of the *cavum arteriosum* and the long-axis systolic diameter of the *cavum pulmonale*. Both obtained values were lower than the significance threshold (<5%). Objectively, in our opinion, the difficult evaluation of the above-mentioned structures may be related to the spongy nature of the ventricular myocardium. The non-spongy nature of the right atrium, pulmonary artery and left aorta walls makes them fixed structures and therefore they are always very easy to identify. Consequently, it is easier to assess their diastolic diameter, which would make it possible to evaluate a possible enlargement of the right atrium and arterial trunks in cases of congenital or acquired diseases.

Regarding the Doppler measurements, the obtained repeatability was excellent, with good image quality. The lack of reference values for this species in the literature makes it impossible that they can be compared. Certainly, the obtained values are consistent with those observed for other species of reptiles, (Rishniw & Carmel, 1999; Schilliger et al., 2003). given the laminar flows at low speed, and mammals. At AV levels, only laminar flows were observed, which allowed us to exclude acquired heart diseases (Schilliger et al., 2003).

In conclusion, echocardiography is a useful, non-invasive diagnostic tool to evaluate the anatomy of the ophidian heart and can contribute to the development of cardiology in reptiles in general. Understanding the normal anatomy and flow is mandatory to improve the ultrasonographer's ability to identify cardiac abnormalities such as congenital heart defects, endocarditis, cardiac neoplasia, thrombi and cardiomyopathy. Once clinicians become familiar with using echocardiography in reptiles, the use of this diagnostic modality will increase in clinical practice and improve the opportunity to obtain diagnoses other than by necropsy, as well as with the evaluation of intracardiac flow, morphology and velocity. The description of a reference range in this study and the certainty of being able to repeat the measurements on all subjects with a certain ease allows us to lay the foundations for the echocardiographic evaluation of this species. Indeed, once a physiological range is obtained, the clinician can thus be able to make in vivo diagnosis with more certainty and therefore propose the most appropriate treatment for the individual subject. Lastly, Doppler echocardiography could be used to assist researchers studying the blood flow patterns of snakes, but it can be a very important clinical indication in subjects who have congenital malformations and who may have changes in the blood flows and shunts. This study is certainly only the beginning of a larger study involving the evaluation of a greater number of subjects and different species. We can affirm that the repeatability obtained in the measurements allows us to propose our data as reference values for *P. regius*.

CONFLICT OF INTEREST

The Authors declare that they have no conflict of interest.

AUTHOR CONTRIBUTION

MARA BAGARDI: Conceptualization; Data curation; Formal analysis; Writing-original draft; Writing-review & editing. **Edoardo Bardi:** Conceptualization; Data curation; Writing-original draft; Writing-review & editing. **Martina Manfredi:** Data curation; Writing-original draft. **Arianna Segala:** Conceptualization; Data curation. **Antonella Belfatto:** Formal analysis. **Stefano Cusaro:** Writing-original draft; Writing-review & editing. **Stefano Romussi:** Supervision; Writing-review & editing. **Paola Giuseppina Brambilla:** Supervision; Writing-original draft; Writing-review & editing.

PEER REVIEW

The peer review history for this article is available at https://publons.com/publon/10.1002/vms3.426.

ORCID

Mara Bagardi https://orcid.org/0000-0002-5247-3796
Edoardo Bardi https://orcid.org/0000-0002-6539-5619

REFERENCES

Barten, S. L., & Frye, F. L. (1981). Leiomyosarcoma and myxoma in a Texas indigo snake. *Journal of the American Veterinary Medical Association*, *179*, 1292–1295.

Bogan, J. E. (2017). Ophidian cardiology – A review. *Journal of Herpetological Medicine and Surgery*, *17*, 62–77.

Conceicão, M. E., Monteiro, F. O., Andrade, R. S., Margalho, V. E., Filho, E. S., Monteiro, M. V., Castro, P. H., Stone, A., Rahal, S. C., & Melchert, A. (2014). Effect of biometric variables on two-dimensional echocardiographic measurements in the red-tailed boa (*Boa constrictor constrictor*). *Journal of Zoo and Wildlife Medicine*, *45*, 672–677.

Divers, S. J., & Mader, D. R. (2006). Section 4 - Medicine 14. Cardiology. In *Reptile medicine and surgery* (2nd ed.). Elsevier Health Sciences.

Frye, F. L. (1991). Snakes. In *Biomedical and surgical aspects of captive reptile husbandry* (2nd ed.). Veterinary Medicine Publishing Co.

Frye, F. L. (1994). Diagnosis and surgical treatment of reptilian neoplasms with a compilation of cases 1966–1993. In Vivo. *International Journal of in Vivo Research (Athens, Greece)*, *8*(5), 885–892.

Goodrich, E. S. (1919). Note on the reptilian heart. *Journal of Anatomy*, *53*, 298–304.

Hochscheid, S., Bentivegna, F., & Speakman, J. R. (2002). Regional blood flow in sea turtles: Implications for heat exchange in an aquatic ectotherm. *Physiological and Biochemical Zoology*, *75*, 66–76. https://doi.org/10.1086/339050

Hruban, Z., Vardiman, E., Meehan, T., Frye, F. L., & Carter, W. E. (1992). Hematopoietic neoplasms in zoo animals. *Journal of Comparative Pathology*, *106*, 15–24.

Jacobson, E. R., Homer, B., & Adams, W. (1991). Endocarditis and congestive heart failure in a XXXbsolet python (*Python molurus bivittatus*). *Journal of Zoo and Wildlife Medicine*, *22*, 245–248.

Jensen, B., Moorman, A. F. M., & Wang, T. (2014). Structure and function of the hearts of lizards and snakes. *Biological Reviews*, *89*, 302–336. https://doi.org/10.1111/brv.12056

Jensen, B., Nielsen, J. M., Axelsson, M., Pedersen, M., Lofman, C., & Wang, T. (2010). How the python heart separates pulmonary and systemic blood pressures and blood flows. *Journal of Experimental Biology*, *213*, 1611–1617. https://doi.org/10.1242/jeb.030999

Jensen, B., & Nyengaard, J. R. (2010). Anatomy of the python heart. *Anatomical Science International*, *85*, 194–203. https://doi.org/10.1007/s12565-010-0079-1

Lillywhite, H. B., & Donald, J. A. (1989). Pulmonary blood flow regulation in an aquatic snake. *Science*, *245*(4915), 293–295. https://doi.org/10.1126/science.2749262

Lillywhite, H. B., & Gallagher, K. P. (1985). Hemodynamic adjustments to head-up posture in the partly arboreal snake, *Elaphe XXXbsolete*. *Journal of Experimental Zoology*, *235*(3), 325–334.

Mattoon, J. S., & Nyland, T. G. (2015). *Small animal diagnostic ultrasound* (3rd ed., pp. 217–331). Elsevier.

Rishniw, M., & Carmel, B. P. (1999). Atrioventricular valvular insufficiency and congestive heart failure in a carpet python. *Australian Veterinary Journal*, *77*, 580–583. https://doi.org/10.1111/j.1751-0813.1999.tb13193.x

Schilliger, L., Tessier, D., Pouchelon, J. L., & Chetboul, V. (2006). Proposed standardization of the two-dimensional echocardiographic examination in snakes. *Journal of Herpetological Medicine and Surgery*, *16*, 76–87. https://doi.org/10.5818/1529-9651.16.3.76

Schilliger, L., Tréhiou-Sechi, E., Petit, A. M. P., Misbach, C., & Chetboul, V. (2010). Double valvular insufficiency in a Burmese Python (*Python molurus bivittatus*, Linnaeus, 1758) suffering from concomitant bacterial pneumonia. *Journal of Zoo and Wildlife Medicine*, *41*, 742–744. https://doi.org/10.1638/2010-0094.1

Schilliger, L., Vanderstylen, D., Piétrain, J., & Chetboul, V. (2003). Granulomatous myocarditis and coelomic effusion due to *Salmonella enterica* arizonae in a Madagascar Dumerili's boa (*Acrantophis dumerili*, Jan. 1860). *Journal of Veterinary Cardiology*, *5*, 43–45. https://doi.org/10.1016/S1760-2734(06)70044-3

Sklansky, M. S., Levy, D. J., Elias, W. T., Morris, P., Grossfeld, P. D., Kashani, I. A., Shaughnessy, R. D., & Rothman, A. (2001). Reptilian echocardiography: Insights into ontogeny and phylogeny. *Echocardiography*, *18*(6), 531–533. https://doi.org/10.1046/j.1540-8175.2001.00531.x

Snyder, P. S., Shaw, N. G., & Heard, D. J. (1999). Two-dimensional echocardiographic anatomy of the snake heart (*Python molurus bivittatus*). *Veterinary Radiology & Ultrasound*, *40*, 66–72. https://doi.org/10.1111/j.1740-8261.1999.tb01840.x

Starck, J. M. (2009). Functional morphology and patterns of blood flow in the heart of *Python regius*. *Journal of Morphology*, *270*, 673–687.

Starck, J. M., & Wimmer, C. (2005). Patterns of blood flow during the postprandial response in ball pythons, *Python regius*. *Journal of Experimental Biology*, *208*, 881–889. https://doi.org/10.1242/jeb.01478

Van Mierop, L. H. S., & Kutsche, L. M. (1981). Comparative anatomy of the ventricular septum. In A. C. G. Wenink, A. Oppenheimer-Dekker & A. J. Moulaert (Eds.), *The ventricular septum of the heart* (pp. 35–46). Matinus Nijhoff Publishers.

Wang, T., Altimiras, J., & Axelsson, M. (2002). Intracardiac flow separation in an in situ perfused heart from Burmese python *Python molurus*. *Journal of Experimental Biology*, *205*, 2715–2723.

Wang, T., Altimiras, J., Klein, W., & Axelsson, M. (2003). Ventricular haemodynamics in *Python molurus*: Separation of pulmonary and systemic pressures. *Journal of Experimental Biology*, *206*, 4241–4245. https://doi.org/10.1242/jeb.00681

Webb, G., Heatwole, H., & de Bavay, J. (1971). Comparative cardiac anatomy of the reptilia. I. The chambers and septa of the varanid ventricle. *Journal of Morphology*, *134*, 335–350. https://doi.org/10.1002/jmor.1051340306

White, F. N. (1968). Functional anatomy of the heart of reptiles. *American Zoologist*, *8*, 211–219. https://doi.org/10.1093/icb/8.2.211

Wyneken, J. (2010). Anatomy and physiology cardiopulmonary systems in reptiles. Proceedings of the Association of Reptilian and Amphibian Veterinarians, 99–106.

Young, B. A., & Saunders, M. (1999). Direct visualization of blood flow through the interaortic foramen in the eastern diamondback rattlesnake, *Crotalus adamanteus*, using echocardiography and color Doppler imaging. *Journal of Experimental Zoology*, *284*, 742–745.

SUPPORTING INFORMATION

Additional supporting information may be found online in the Supporting Information section.

How to cite this article: Bagardi M, Bardi E, Manfredi M, et al. Two-dimensional and doppler echocardiographic evaluation in twenty-one healthy *Python regius*. *Vet Med Sci*. 2021;00:1–9. https://doi.org/10.1002/vms3.426